Metal recovery by electrodeposition from a molten salt two-phase cell system

Tazdin Amietszajew[1*], Seetharaman Sridhar[1], Rohit Bhagat[1]

[1]WMG, University of Warwick, Coventry CV4 7AL, UK

*T.Amietszajew@warwick.ac.uk

ABSTRACT

A novel electrochemical recovery method of Co, Cu, Mn and Ni from a reactor based on two immiscible molten phases, to enable selective metal plating, sufficient feedstock dissolution and protection from re-oxidation, was designed and characterised through voltammetry and chronoamperometry. The immiscible phases in the electrolytic cell were NaCl and Na_2O-$2B_2O_3$ at 1173 K, and the metal feedstock to be recovered was either metal chlorides or metal oxides of Co, Cu, Mn and Ni. Metals could be successfully recovered as plated metal deposits and the formal redox reaction potentials were reported. Metals thermodynamic behaviour differences between the cells were analysed. Analysis of the metal deposits showed that the recovered metals were of high purity (~99%). This offers an alternative method to recycle valuable metals present in the growing e-waste stream.

I. Introduction

Despite the constant improvements in the metal processing technology, valuable metals recovery from scrap and e-waste stream is still lacking. Recovery of such metals is of high interest both in EU[1] and USA[2] when considering a foreseeable constraints in raw materials availability and energy costs of extraction in a future society. In the US alone, each year at least 94 million USD worth of non-ferrous metals are disposed of as land-fill[3], while the global e-waste recycling rate was estimated to be less than 20% in 2009[4], in part due to lack of relevant recycling technology. Rapid development of Li-Ion and NiMH battery technology causes increased consumption of Co, Cu, Mn, Ni, Zn and Li[5–7], with Li-Ion cells (together with NiMH) accounting for over 80% of the rechargeable batteries market[8]. Methods currently available for these metals recovery are adapted pyro- or hydro-metallurgical[9] minerals processing operations[8]. As a result, not being originally developed for this purpose, these methods cause losses of raw material or ignore specific metal streams altogether, e.g. recovering some and slagging other elements[8]. Additionally, the majority of these processes produce significant amounts of water waste, relying on leeching or other water-based solutions. Such methods requires highly corrosive acids use, which are environmentally damaging and contaminate the waste water heavily, including sulphates by-products presence[10–13]. For these reasons, new metal recovery methods research is necessary for the technological development and as an alternative to the existing processes.

Additional stream of rare and valuable metals is possible in form of metal hyperaccumulating plants. A range of plants (e.g. fungi, some wild plants) was reported to be capable of removal of heavy-metal from contaminated soil (e.g. near roads). This way the soil can be cleared for revitalisation, while metals are concentrated in the plant roots and shots. Such plants are then incinerated, and the metal-rich powder requires post-processing for metal recovery[14,15].

Molten salts present an alternative to water based metal processing methods, and are already used in a diverse range of processes, such as extraction[16], purifying[17] and coating[18]. Technical barrier towards developing an electrochemical based recovery process include: achieving sufficient dissolution of the metal in the electrolyte and the re-oxidation of the metal after winning. A further technical challenge is the selective winning of various elements from a feedstock. Using a two phase system could solve the difficulty of dissolving the metal feed efficiently and without a need for expensive atmosphere control, while retaining electrochemical properties and cleanliness of the second phase. The method presented in this article uses molten borates, known mainly for boriding[19,20] and glass forming[21,22], and molten chlorides, widely used in electrochemistry (electrodeposition[23], alloy formation[24] and nano-structured carbon materials formation[25]. However, the thermodynamic properties of molten salts are by far less understood than water-based chemistry. Currently and at the moment of writing this article the literature and information regarding thermodynamics of specific molten salt systems is scarce[26].

Borates has been partly studied for their high metal solubility application in metal extraction[27]. Furthermore molten borate and molten chloride has been studied as immiscible phases[28]. It has been suggested that borates are capable of dissolving significant quantities of metal species, and presents a feasible basis for metal recovery process. As the borates are thermodynamically stable oxides, they can work in open atmosphere without risk of reaction with moisture or oxygen in the air. Any impurities in the feedstock in contact with borates melt would safely dissolve into the melt or pyrolyse due to the high temperature of the molten salt.

Chloride salts can be used for a range of metals electrodeposition processes, e.g. for Ti[29], Al-Nb[30], Mg, Ce and Li[24], Ag[31], and many others, including metals from the f-block[32]. The use of molten chlorides in

electrochemistry requires atmosphere control (neutral gases) and additional control measures due to possible salt evaporation[33] and chlorine formation.

The process proposed is based on a liquid-liquid extraction, essential step possible thanks to the immiscibility phenomenon common for the molten alkali borates and molten halides systems. This is due to the highly polymeric nature of molten borate, in contrast to purely ionic structure of the latter[34,35]. The molten salts liquid-liquid interface transfer mechanism was previously reported in the literature[28].

Considering the economical side of the process, it offers certain benefits over hydrometallurgical methods. The process proposed uses two salts (sodium chloride and borax) for the bulk of the cell, which are naturally occurring and quite prevalent[36,37]. This removes the adverse environmental impact of heavily corrosive and expensive acids use (e.g. sulfuric acid, hydrofluoric acid), which is an issue when hydrometallurgical processes are considered[11]. This also allows for zero water waste process, when the contaminated water disposal is a growing financial factor and under the pressure of the pro-ecological approach and governmental incentives to reduce the waste output. Regarding the feed pre-treatment, hydrometallurgical methods require small particle size for the leeching to reach required concentrations[12,38] which adds the milling step and quite often thermal pre-treatment, while the evaluated method can efficiently work on pellet-size metal sources even without any additional mixing.

Metal recovery can be highly beneficial, as it is one of the most profitable processes in the waste treatment industry[39]. It is evident that the largest part of the evaluated process cost would be the heat-generation for the melt and electricity cost for the electrolysis, making the price-per-mass-unit of the recovered metal relatively high. However, with proper engineering design the process could partially rely on the residual heat widely present in the metal industry. Furthermore, while currently electricity prices would make the method rather expensive, the electricity cost would be driven low by other research sectors, i.e. nuclear and renewable sources, promoting electrolysis based systems. Additionally, with the development of the process and the metal industry needs, the benefits of complete and diverse metals recovery and wide range of possible feedstock would potentially outweigh the cost, especially including the increasing waste disposal rates and limitations.

This study focuses on the recovery of the Cu, Co, Ni and Mn metal, constituents in spent batteries, from the borate-chloride two-phase molten salt system at 1173 K. Experiments have been carried out in both single (chloride) and two-phase (borate-chloride) salt systems, in a test set-up specifically designed for molten-salt electrolysis. Transient electrochemical techniques like cyclic voltammetry and chronoamperometry have been used for the electroreduction and process evaluation, as well as energy dispersive X-ray spectroscopy, inductively coupled plasma optical emission spectroscopy and X-ray diffraction for the analysis of the processed materials.

The objective of this study was to assess whether the sodium borate-chloride system is capable of providing the metal ions from the borate phase, while retaining the positive electrochemical attributes of the sodium chloride layer, i.e. electrolytic stability, and to compare the system to a single-phase sodium chloride cell. Such a combination would allow for the recovery of high purity metal by electrowinning from chloride salt, while using various metal sources as the feed for the dissolution in sodium borate.

II. Methods

Test set-up

The electrochemical experiments were carried inside a vertical tube furnace, in a set-up presented in Figure 1. The tests were conducted inside a gas-tight Inconel® tube with argon atmosphere, allowing for O_2 levels as low as 50ppm. An alumina crucible (Coors™, high-alumina crucible, 100ml) was used to contain the melt which consisted of 35g of sodium borate (Na_2O-$2B_2O_3$, *Sigma-Aldrich®, anhydrous, >98.0 %*) and 65g of sodium chloride (NaCl, *Sigma-Aldrich®, Redi-Dri™, anhydrous, >99 %*). A metal oxide pellet (~10g) was inserted at the bottom.

The borate salt layer was saturated with the feed prior to the test, and subsequently allowed to equilibrate with the molten chloride layer for at least 1h before testing. The process is mainly diffusion controlled as is discussed later in the article, however partial heat convection is plausible promoting faster equilibration. Due to the density differences, the chloride salt (1.50 g/cm^3)[40] was on top of the borate (2.06 g/cm^3)[41] layer, which with the mass differences resulted in the chloride layer being twice the height of the borate phase, allowing for easier electrode placement. The oxides selected for the experimentation were the most stable oxides of their respective metals at the test temperature (1173 K)[26,42]. Depending on the test conducted, the metal oxide was one of the following: NiO (*99,8 %*), Co_3O_4 (*99,5 %*), CuO (*98 %*) and Mn_2O_3 (*99 %*) from *Sigma-Aldrich®*.

Alternatively, in case of the single-phase chloride-only set-up, the crucible was filled with 70g of sodium chloride (NaCl) and the respective stable metal chloride: $NiCl_2$ (*>99.0 %*), $CoCl_2$ (*>99.0 %*), $CuCl_2$ (*>99.0 %*) or $MnCl_2$ (*>99.0 %*) from *Sigma-Aldrich®* at 1 wt% for the comparativeness of the tests. All the metals were tested separately in this study. The electrodes were lowered into the melt through insulating Macor® ceramic fittings.

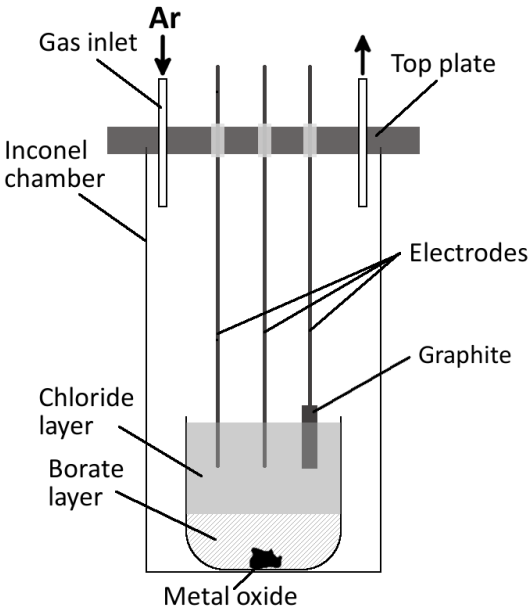

Figure 1 Electroplating set-up

Electrodes used in the process were selected depending on their thermal and corrosion resistance, low thermal expansion and chemical resistance[43–47]. The working electrode (*WE*) was a tungsten rod (2mm diameter), Counter Electrode (*CE*) was a graphite cylindrical block (6mm diameter) on a stainless steel current collector. A tungsten rod (2mm diameter) was adopted as a quasi-reference electrode to avoid introducing impurities. The electrodes surface area in contact with the electrolyte was dependable on the immersion depth (as visible in Figure 1) and varied around 0.3cm^2. The electrodes were placed in line in equidistance to the reference electrode, with ~1.7cm gaps between them. The metal surfaces were cleaned and polished with successively finer grades of sand paper until a mirror-like surface was obtained before every test. The graphite blocks were treated as one-use consumable to avoid cross-contamination.

Electroplating

Metal oxide pellets formation and dissolution has been explained in a previous publication by the authors[27]. The assembly was dried in the tube furnace for 24 hours at elevated temperature before the test. After filling the chamber with argon, the experimental temperature of 1173 K was achieved (at the rate of 10 K/min) and 30 minutes were given to ensure equilibration.

To observe the electrochemical reduction reaction kinetics, cyclic voltammetry (CV) was applied at 100 mV/s scan rate. The analysis of current/voltage curves provides essential information about the process dynamics and step characteristic[48,49]. The obtained experimental potential values were compared against the thermodynamic values for the better understanding of the system. Metals for the analysis were deposited on the negative electrode potentiostatically, at the potential value higher than the peak value obtained with the use of CV, in order to ensure the removal of the initial surface concentration of the reagent[50].

Post-mortem analysis

X-EDS

After the potentiostatic process the electrodes were lifted from the melt and cooled down under argon atmosphere to limit re-oxidation. The metal-plated end of the electrode was cut off using precision saw, and analysed using FEG-SEM (Carl Zeiss Gemini®) with X-ray Energy Dispersive Spectroscopy (X-EDS, Oxford Instruments®). The chemical identification is based on the energy of the X-rays emitted, while quantification is possible due to the detection peak intensity being related to the chemical concentration[51].

X-ray Diffraction

The salt remaining after the process was extracted from the crucible mechanically, then crushed and ground down to a fine powder. Because the interface between the two immiscible phases remains clearly defined, it is easy to break the layers apart. While the borate salts are forming a glass phase, chloride layer is highly crystalline. For this article the database COD (Crystallography Open Database) was used for phases identification. The instrument used was PANalytical Empyrean X-ray Diffractometer with a cobalt source. The scan was evaluated on a spinning stage in a range of 8-100 2θ angles, using Cobalt X-ray source.

III. Results and Discussion

Electrolysis would occur in the top chloride layer of the cell shown in Figure 1 according to the following reactions:

$$Cathode: \ Me_{(l)}^{x+} + xe^- = Me_{(s)} \quad (1)$$

$$Anode: \ xCl_{(l)}^- = \frac{x}{2} Cl_{2(g)} \uparrow + xe^- \quad (2)$$

$$\text{Cell:} \quad MeCl_x = Me_{(s)} + \frac{x}{2} Cl_{2(g)} \uparrow \quad (3)$$

In the single phase system, these would be the only occurring processes. The overall process happening in the two-phase system, in addition to the reactions above requires dissolution of the oxides in the oxide melt, transport to the oxide/chloride interface, transfer across the oxide/chloride interface and transport in the chloride electrolyte to the electrode. The metal oxides (CuO, Co_3O_4, Mn_2O_3 and NiO) solubility in borate melts study was completed by the author previously[27] and it was established that the addition of Na_2O to the melt resulted in 6-23% dissolved metal oxides. The focus of this study is to analyse the electrolytic cell as a whole, and compare the single- and two-phase molten salt systems.

Electrochemical analysis

Plating of all the evaluated metals was conducted, and the Cyclic Voltammetry profiles of the redox reactions were obtained versus reference electrode. The reduction peaks recorded are within the electrochemical stability window of the melt [-1.5V to +0.5V vs Ref] shown in Figure 2, allowing for the metals recovery. The CV scans shows the reduction and oxidation peaks, confirming the reversible nature of the electroplating process in the presented system, and allowing for the formal potentials analysis. The flat plateau preceding the peak is attributed to the reaction kinetic barrier, while the CV peak tailing corresponds to the diffusion controlled area[52].

The Cyclic Voltammetry profiles are presented in Figure 3 (for single-phase cell) and Figure 5 (for two-phase cell). As the chlorine gas evolves readily at positive potentials, as described by reaction (2), when scanning the positive potential values region the electric current rates can be altered by this process. The formal redox potential values are listed in Table 1 and Table 2, followed by the analysis. The single-phase cell system was used for the correlation of the experimentally obtained values with the thermodynamic data, and to enable comparison with the two-phase system.

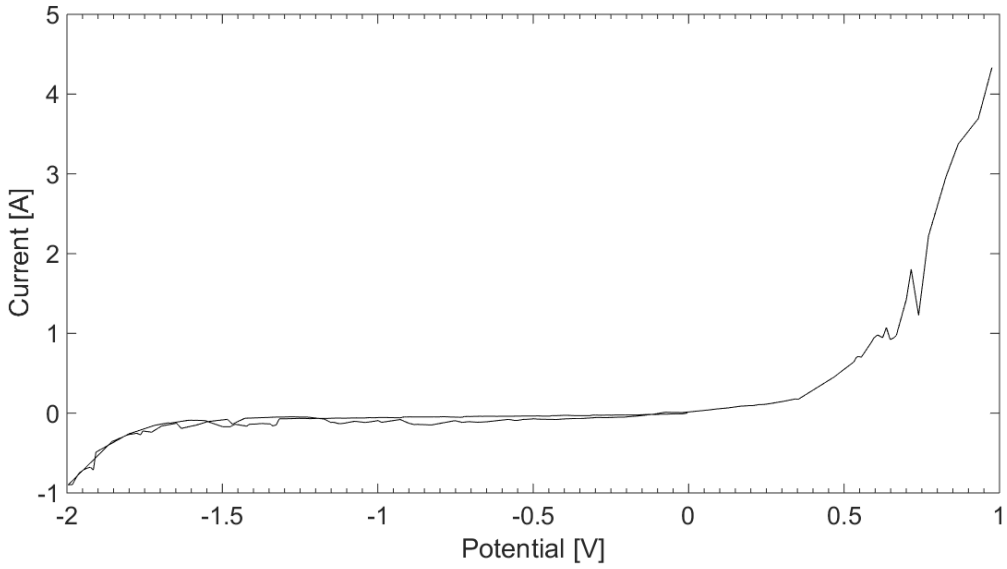

Figure 2 Electrochemical stability window of the cell setup studied

Single-phase (NaCl) cell:

Experimental data for the single-phase cell setup is presented in Table 1 and shown against calculated thermodynamic values of the metal chloride electrolysis (reaction 3) at 1173 K, with the analysis following the table. The current-voltage plots obtained are shown in Figure 3. The values of electrolysis potential were calculated using the Gibbs free energy and cell potential relation equation (4):

$$E = \frac{-\Delta G}{nF} \tag{4}$$

where: ΔG is the Gibbs free energy change [*J/mol*], E is the calculated potential [*V*], *F* is the Faraday constant [*C/mol*], and *n* is the number of electrons exchanged during the reaction.

The metal chloride concentration was similar across all samples for the comparativeness of the tests, set at 1 wt% which translates to: 0.121M Co, 0.116M Cu, 0.1249M Mn, 0.1213M Ni). The experimental values shown in the table are relevant to the metal plating reaction (1) versus the W reference in the experimental set-up at 1173 K. The calculated thermodynamic metal chloride electrolysis values are relevant with reference to the chlorine formation occurring at the positive electrode, as is reflected by the cell reactions (1-3).

Table 1 Experimental and thermodynamic values of electrolysis in sodium chloride melt, in a single-phase (NaCl) cell with metal chloride as the feed.

NaCl + Me_xCl_y				
single-phase cell	**Co**	**Cu**	**Mn**	**Ni**
Formal redox potential [V] experimental, (vs. W ref)	0.050	-0.182	-0.651	0.094
Thermodynamic potential [V] calculated, (vs. Cl_2 evolution)	-0.949	-0.418 Cu(II) -1.075 Cu(I)	-1.860	-0.737

The values obtained show a similar tendency as reported by Gaur et at.[53], although he evaluated a considerably different molten chlorides system. In the system evaluated in this article a number of overpotentials can be expected. This includes the *activation overpotential* (E_{act}) often called reaction overpotential (caused by the activation energy necessary to transfer the electron between the electrode and the electrolyte), *concentration overpotential* (E_{conc}) which accounts for the depletion of the reactant at the electrode surface (and includes the diffusion overpotential), and *resistance overpotential* (E_{Ω}), which includes junction overpotential, electrode capacitance and are specific to each cell design. To minimise these effects, the formal potential of the redox reactions was analysed.

It is clear from the experimental data and visible in Figure 3 that the reduction potential of copper is more negative than that of cobalt, which is counter-intuitive when compared to the thermodynamic data, as the decomposition of $CuCl_2$ requires less energy than of $CoCl_2$. There are two possible reasons behind this observation. The simple answer would be the overpotential of copper electrodeposition on tungsten, e.g. nucleation overpotential, caused by the electrode material and its structure[47,50,54]. Alternative phenomenon causing this behaviour would be that copper chloride being a mild oxidant can react according to the reaction (5), especially in reducing atmosphere at the elevated temperature[42]. This would result in Cu^{1+} ion present in the melt, explaining the more negative metal electroplating potential observed.

$$CuCl_2 = CuCl + 0.5Cl_2 \tag{5}$$

The thermodynamic value of the copper(I) chloride electrolysis potential under the test parameters equals -1.075 V, which complements the trend of the experimental data when used in place of the copper(II) chloride, as shown in Table 1. The above assumption was experimentally evaluated using copper(I) chloride for the electrolysis, which resulted in a similar plating behaviour observed. Based on the thermodynamic calculations and experimental confirmation, it was concluded that the electrolysis process observed was indeed of the copper(I) chloride.

The difference between the thermodynamic values of metal chloride electrolysis reaction (3), and the experimentally measured formal metal redox reaction potentials can be ascribed to the W reference electrode shift and the anodic reaction (2) occurring during the electrolysis. The relation was found to be linear, as shown in Figure 4, and is described mathematically. This allows for calibration of the evaluated system using the correlation between the thermodynamic electrolysis values and the experimentally measured formal redox reaction (1) potentials, as described with the following empirical equation (6):

$$E = E_{measured} * 1.410 - 0.912 \quad (6)$$

where: E is the thermodynamic electrolysis potential [*V*] and $E_{measured}$ is the formal redox reaction potential recorded [*V*].

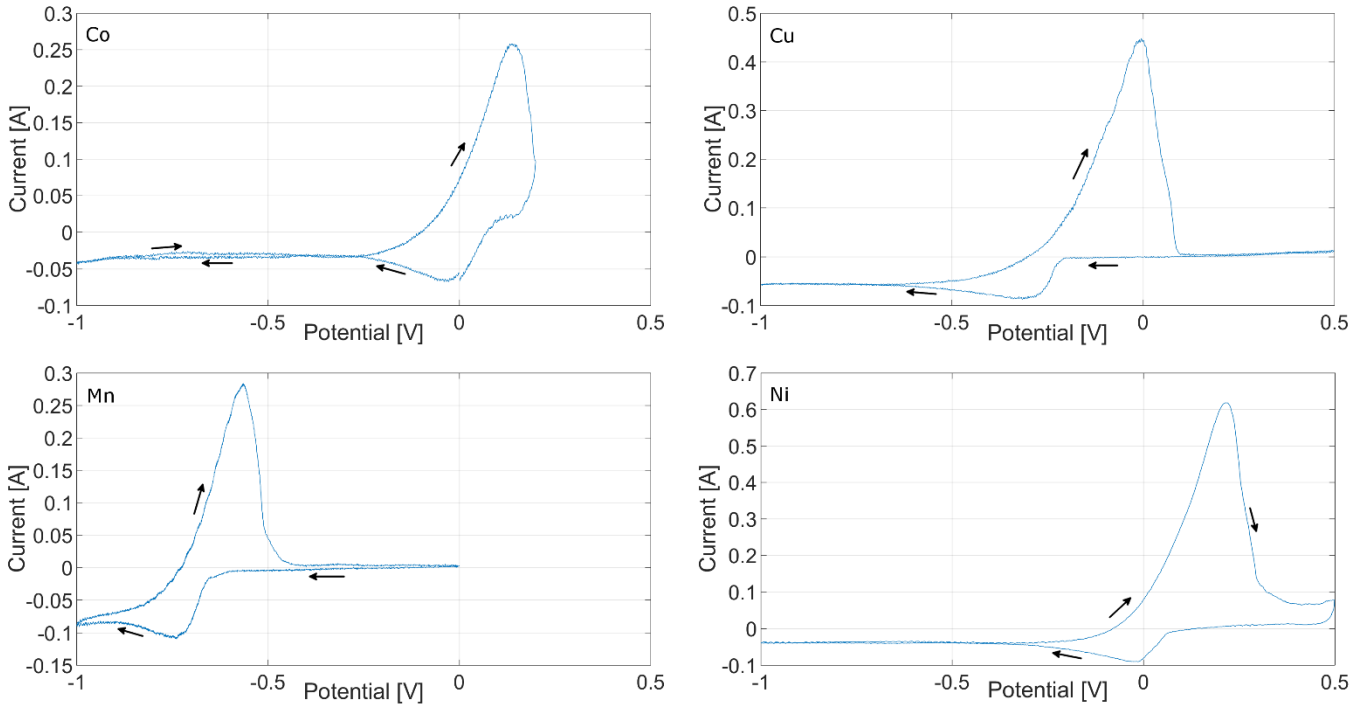

Figure 4 Voltammograms of the metal chlorides electroreduction from the single-phase (NaCl) cell setup at 1173 K. Scan rate 0.1 V/s. Arrows indicate the direction of the scan.

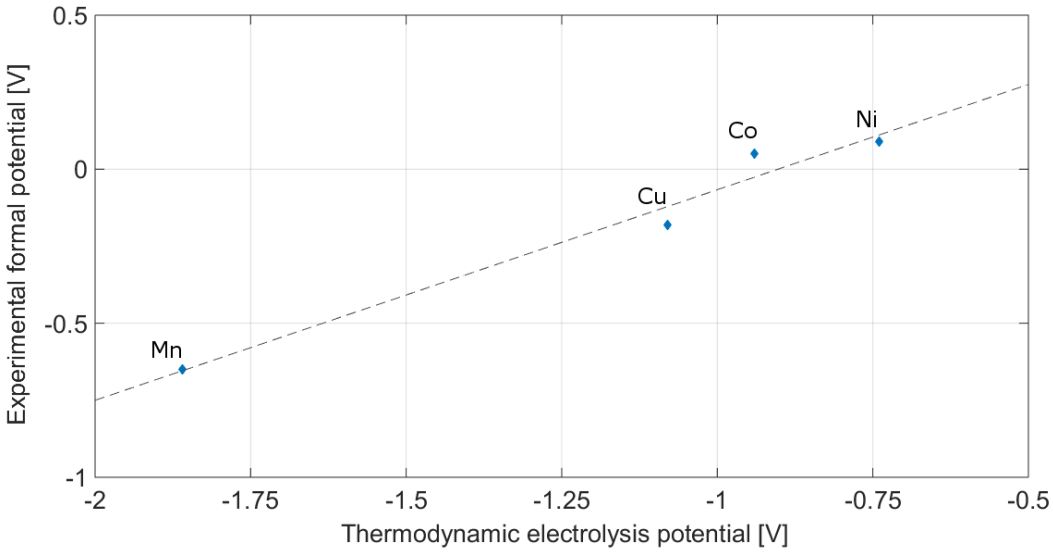

Figure 3 Thermodynamic and experimental redox reaction potentials correlation.

Two-phase (Na_2O-$2B_2O_3$ + NaCl) cell:

The second set of experiments was conducted in the two-phase (Na_2O-$2B_2O_3$ + NaCl) cell setup, using the same test parameters. Metal oxides (Co_3O_4, CuO, Mn_2O_3 and NiO) were used as the feed and were located in the borate phase (at the bottom of the test crucible). An exchange mechanism reaction (7) describing the metal ions transfer from borate to chloride phase has been proposed by Williams et.al.[28], which describes the chemical reaction driving the ionic exchange feeding the metal into the chloride layer. The metal ions remain at their initial oxidation state according to the interface transfer reaction. This mechanism is the closest explanation available in the literature at the time of writing this article.

$$MO_{(s)} + 2NaCl_{(l)} + B_2O_{3(l)} = MCl_{2(l)} + 2NaBO_{2(l)} \quad (7)$$

As the mix composition was within the wide area of immiscibility gap between the two (borate and chloride) phases, the layers were clearly divided by liquid-liquid interface and could be easily separated after the testing by breaking apart. The mutual solubility of the evaluated phases is reported to be very low [34,55], and was measured using Inductively Coupled Plasma – Optical Emission Spectrometry (ICP-OES). A piece of metal deposit encapsulated within the solidified upper-phase salt (NaCl) droplet was analysed, and the boron amount was found to approximate 40 ppm, which is of little effect on the process considered, confirming the separation of the phases.

The sodium borate salt used in this experiment has a significant number of negatively charged exchange sites (the abundance of which depends on the alkali metal proportion to the boron oxide matrix)[34], resulting in the metal cations selectivity and preference shifted towards the borate phase. Therefore, the partition coefficient is significantly biased towards the borate layer limiting the concentration of the metal ions in the chloride phase. The metal concentrations in the sodium borate phase were evaluated by the author in previous publication[27], and were reported as follows: Cu 12 wt%, Co 14.7 wt%, Mn 13.2 wt% and Ni 4.0 wt% (σ-0.1). The values of metal concentrations achieved in the chloride layer were measured using the X-EDS, and were as follows: (Cu 3 wt% (σ-0.2), Co 0.7 wt% (σ-0.1), Mn 0.4 wt% (σ-0.1) and Ni 0.1 wt% (σ-0.1)). However, due to copper reaching high concentration and changing the characteristics of the mix by superimposition of the electron component of the ion resulting in ion-electron conductivity[56], soft-shorting phenomenon was observed and in order to obtain a clear reduction characteristics, the concentration was brought down to 0.5 wt% of copper in the chloride layer.

The metal deposition process, cell and electrodes setup remained identical to the single-phase case. To analyse the difference between the single-phase and two-phase electrochemical behaviour, the samples should be analysed case by case. Table 2 represents the experimentally obtained formal redox potentials, adjusted using the equation (6) to enable comparison with the metal chloride electrolysis values from Table 1 (single-phase cell setup).

Table 2 Experimental values of electrolysis in the two-phase (Na_2O-$2B_2O_3$ + NaCl) cell with metal oxides as the feed. The revised values were obtained using equation (6) for thermodynamic comparison with the single-phase cell system.

NaCl + Na_2O-$2B_2O_3$ + Me_xO_y				
two-phase cell	**Co**	**Cu**	**Mn**	**Ni**
Formal redox potential [V] experimental, (vs. W ref.)	0.127	-0.273	-0.454	-0.583
	-0.663	-1.037		
Revised formal potential [V] calculated, (vs. Cl_2 evolution)	-0.733	-1.297	-1.552	-1.734
	--1.848	-2.375		
Single- vs two-phase cell electrolysis difference [V]	0.216	-0.222	0.308	-0.997
	-0.899	-1.300		

The shifts between the single- and two-phase cell reduction potentials is likely caused by the lower metal ion amount changing the thermodynamic values (as in the Nernst equation) and due to the different metal cation availability and diffusion from the borate and through the liquid-liquid interface, but could be also rely on the chemistry change. The influences can be listed as follows:

- Concentration difference
- Metal ion state in the chloride
- Mass transfer in the borate layer
- and through the interface

Due to their significant differences, each metal is analysed separately. Nickel metal is the simplest case, as it exists in a +2 oxidation state as a stable chloride and oxide, and forms similar electroreduction profile in both cases. However, the reduction potential shift observed is significant. One needs to keep in mind that the concentration of around 0.1% implies relatively big error margin, and as nickel oxide shows lowest solubility in the borate layer[27], it could be that the ion concentration has a major impact on the reduction potential. Furthermore, as the analyte could be easily depleted from the chloride layer due to its very low concentration, it relies heavily on the borate layer providing the cation, which adds the element of the diffusion through borate and the liquid-liquid interface in order to supply the metal for electrolysis. Reaction mechanism should stay the same, as there is no difference in the metal ion state. In other words, the more negative formal potential values are mostly caused by the limitations of the metal ions availability, mass transfer in the borate layer, and transfer through the interface.

Manganese exists as a stable Mn_2O_3 oxide at the process temperature of 1173 K, which results in a different ion being present in the melt. As an effect, a less-negative formal potential was recorded during the electroplating, as shown in Table 2. Therefore, despite lower concentration of the metal cation, electroreduction potential shift towards the more positive values was observed. This creates

the possibility of manganese being reduced from its +3 oxidation state in the chloride layer. However, no thermodynamic data on the Gibbs free energy of formation of $MnCl_3$ was available as of the time of writing this article. Because of the different ion being present in the single- and two-phase cell setup, the observation of other influences is challenging. Nonetheless, concentration higher than that of Ni implies smaller concentration effect, yet it is still lower than in the single-phase cell. Similar electrolysis profile implies analogous electrochemical reaction occurring at the electrode. The shift places the electroplating peak closer to the Ni reduction value, making them potentially more difficult to separate if both were present in the mix, however the issue could be solved by engineering solutions, like high-overpotential electrodes or alloying mechanisms.

Unique behaviour of peak splitting can be observed during the copper reduction from the two-phase cell, when compared against the single-phase (NaCl) cell sample. This results in two separate peaks, one relatively close to the original value, and second one shifted more into the negative potential values. Such a phenomenon can be explained by either a transient presence of the Cu^{2+} ions together with the Cu^{1+} soon after the interface transition from borate, or alternatively by the formation of oxychlorides. Copper oxychlorides have been previously reported in molten salts, e.g. as a result of copper chloride absorbing oxygen[54], as show in the reaction (8) below.

$$Cu_2Cl_2 + \frac{1}{2}O_2 \leftrightarrow Cu_2OCl_2 \quad (8)$$

Oxychlorides were indeed detected in the sample after processing. The oxychloride identified with the use of XRD in this case was $Cu_4O_4Cl_4$. The difference in the oxychloride formed comes from the copper oxide (CuO) being the precursor instead of copper chloride, and a different chemical reaction happening across the molten salts interface. However, the mechanism behind the formation of oxychlorides from metal oxides during the liquid-liquid interface transfer is not explained by the assumed exchange reaction proposed by Williams et.al. [28] (described earlier in the article). This phenomenon results in the change of the voltammetry profile, suggesting two separate electroreduction reactions. No oxychlorides were detected in case of other metals (Co, Mn and Ni), which is in agreement with their respective CV profiles.

Cobalt is, similarly to manganese, present at a different oxidation state in the two-phase setup than in the single-phase cell, although in this case the oxide stable at the process temperature of 1173 K is a spinel compound with +2 and +3 oxidation states (Co_3O_4), also written as $Co^{II}Co^{III}{}_2O_4$ or $CoO\text{-}Co_2O_3$. The presence of both oxidation states in the chloride phase is reflected in the voltammetry scans, showing two separate peaks. The E values would be different for the additional +3 cobalt ion, otherwise absent in the single-phase cell setup. However, the thermodynamic data on the component present in the chloride phase is scarce, hindering the thermodynamic calculations. If we assume the more negative redox values as the +2 cation reaction, as it is more difficult to reduce than the +3 cation, we are again observing a shift towards the more negative values when compared to the single-phase cell. This could be also partially attributed to the lower reactant concentration, as the measured amount of cobalt in the sample (0.186 M) has to be divided between the two ions, resulting in a theoretical concentrations of 0.062 M for Co^{+2} and 0.124 M for Co^{+3} species.

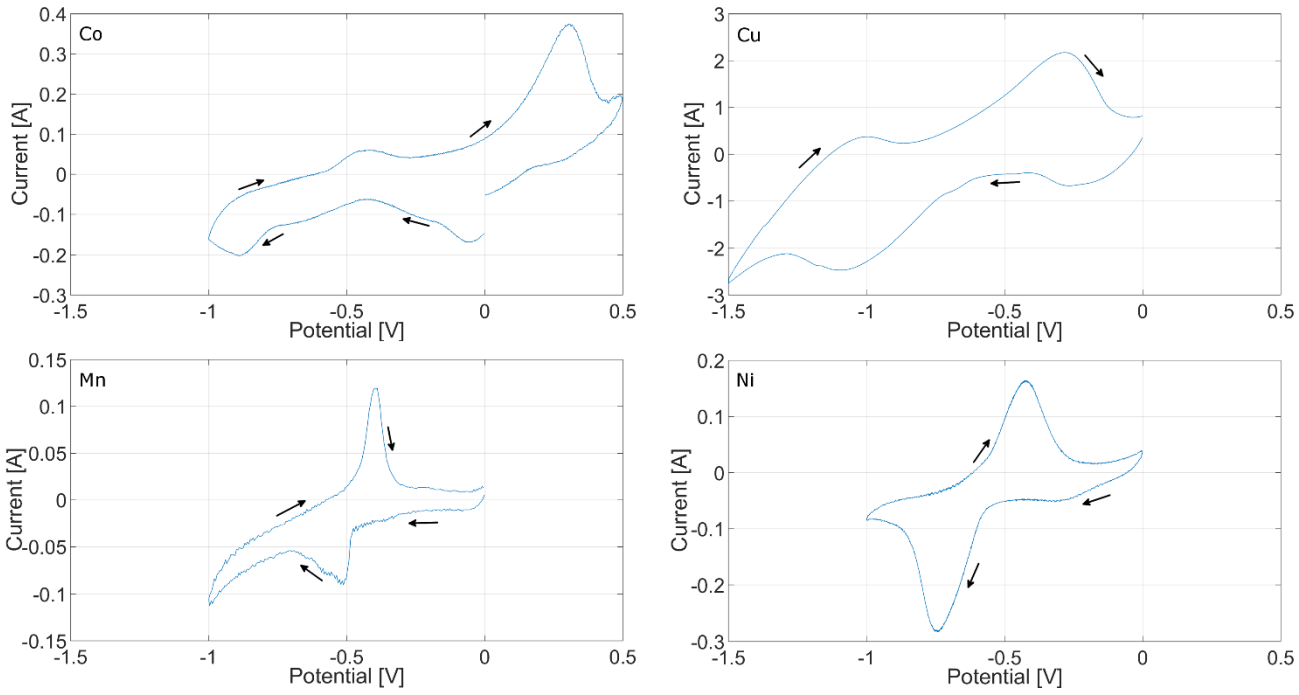

Figure 5 Voltammograms of the metal oxides electroreduction from the two-phase (Na2O-2B2O3 + NaCl) cell setup at 1173 K. Scan rate 0.1 V/s. Arrows indicate the direction of the scan.

In summary, when we compare single- and two-phase cell setups, concentration influence changes in all cases and, apart from Nickel sample, so does the chemistry of the ion resulting in different E value. Mass transfer from the borate layer and through the liquid-liquid interface add to the observed effects. Cobalt and Manganese are at a different oxidation states in single- and two-phase cell, due to their stability as certain oxides at the test temperature of 1173 K, which results in a change of their chemistry and E value. This creates an interesting opportunity to reduce different metal ions from the chloride than the usual metal chlorides available. Lastly, copper shows unique differences due to its oxychlorides formation capability, forming a different component in the chloride layer when transferred from the borate phase. This allows for an alternative metal recovery process, depositing a range of metals, including but not limited to these present in li-ion batteries, from their various oxidation states.

Plated material analysis

Plated metal purity was approximated using a FEG-SEM X-EDS. Due to the microscopic size of the deposits, this method allowed for structural and chemical analysis, and as the ICP-OES analysis confirmed that the retrieved samples contain negligible amounts of boron, the evaluated chemical elements fall within detection capabilities of X-EDS. It was confirmed that the metal was plated with the purity of at least 98% for Cu, 99% for Co, 99% for Mn and 99% for Ni. Metals for the analysis were deposited potentiostatically, with the potential value more negative than the peak value to ensure the removal of the initial surface concentration of the reagent[50]. Figure 6 a) shows an example of amperogram produced during the constant potential electrowinning process of cobalt from the two-phase (Na_2O-$2B_2O_3$ + NaCl) cell.

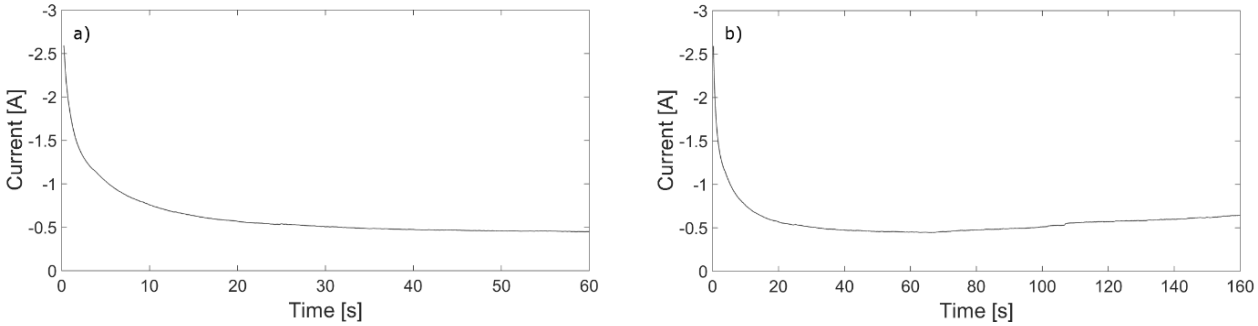

Figure 6 Amperogram of the electroreduction of cobalt from the molten salts system at 1173 K at -660 mV. WE: tungsten, CE: graphite, QRE: tungsten.
a.) Short plating (60 sec.), and b.) Longer plating (160 sec.), with visible current increase over time.

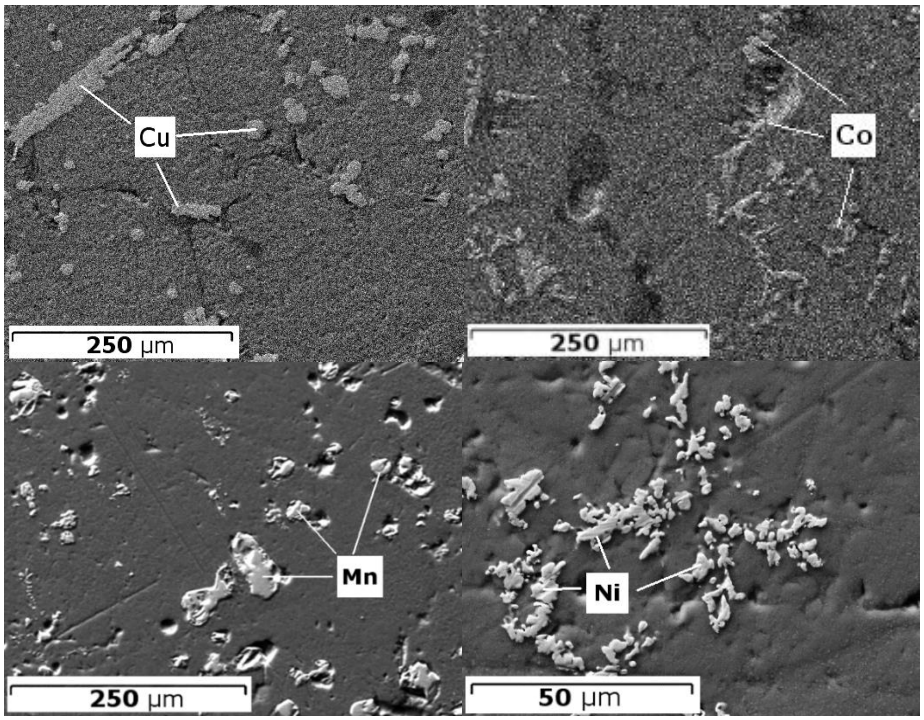

Figure 7 FEG-SEM image of the plated metals. Metal fragments are visible across the chloride in proximity to the electrode.

In case of longer metal electrodeposition (as in Figure 6 b), we can observe the chronoamperogram slowly falling towards the higher current values. This is due to the increasing electrode surface, caused by the high porosity of the deposited metal[57]. Complex deposit structure is also indicated in the FEG-SEM pictures (Figure 7) showing a cross-section of the metals plated. Fragments of electroreduced metal seemingly separated on the planar view suggest more complex structure in the plane perpendicular to the visible surface, trapping the chloride salt in between the metal dendrites. Such structure is also a confirmation of the diffusion control of the process, which fits with the observations other researchers have made in this field[50,57,58].

IV. Conclusions

The objective of this study was to assess whether high purity metals can be recovered by electrowinning from molten salt two-phase (Na_2O-$2B_2O_3$ + NaCl) cell system at 1173 K, and what is the thermodynamic behaviour of said metals in the two-phase melt when compared to a single-phase (NaCl) cell. The electrolysis was conducted on tungsten cathode in a three electrode system. Using the scan rate of 0.1 V/s, voltammograms were plotted for the purpose of identification of the formal redox reaction potential values. The formal redox reaction potentials were reported for the following feedstock: Co_2O_3 [-0.733 /- 1.848 V], CuO [-1.297/-2.375 V], Mn_2O_3 [-1.552 mV] and NiO [-1.734 mV] versus chlorine evolution. Each metal showed different thermodynamic behaviour and was analysed separately in this article. Metals were deposited potentiostatically, and the deposited materials analysed. The SEM scan of the deposited metal suggests heavily dendritic structure, which supports the assumption of the diffusion controlled process. The purity values obtained for the metals plated were approximated as follows: >98% for Cu, >99% for Co, >99% for Mn, and >99% for Ni. The experiments conducted showed that such a setup works for the metals considered (Co, Cu, Mn, Ni), and provides a recovery process alternative to single-phase or aqueous electrowinning methods, removing many issues related to the hydrometallurgical methods (i.e. water waste, toxic acids use, etc.) for these and other valuable metals. Method reported is in an early stage of development reported as a proof-of-concept, and would require additional engineering solutions regarding metals separation in some of the cases evaluated. Evaluated setup could work with e-waste stream, as well as other metal sources (e.g. metal-accumulating biomass).

References

1. European Commission DG Enterprise and Industry. *Critical raw materials for the EU - Report of the Ad-hoc Working Group on defining critical raw materials*. (2010).
2. U.S. Department of Energy (DOE) Office of Policy and International Affairs. *Critical Materials strategy*. (2011).
3. Sunk, W. Survey of metal recovery in the USWTE industry. in *Nawtec 15 Proc. 15th Annu. North Am. Waste to Energy Conf.* (2007).
4. Jiang, P. *et al.* Improving the End-of-Life for Electronic Materials via Sustainable Recycling Methods. *Procedia Environ. Sci.* **16,** 485–490 (2012).
5. Väyrynen, A. & Salminen, J. Lithium ion battery production. *J. Chem. Thermodyn.* **46,** 80–85 (2012).
6. Scrosati, B. & Garche, J. Lithium batteries: Status, prospects and future. *J. Power Sources* **195,** 2419–2430 (2010).
7. Gaines, L. & Cuenca, R. *Costs of lithium-ion batteries for vehicles*. (2000). doi:10.2172/761281
8. Al-Thyabat, S., Nakamura, T., Shibata, E. & Iizuka, a. Adaptation of minerals processing operations for lithium-ion (LiBs) and nickel metal hydride (NiMH) batteries recycling: Critical review. *Miner. Eng.* **45,** 4–17 (2013).
9. Georgi-Maschler, T., Friedrich, B., Weyhe, R., Heegn, H. & Rutz, M. Development of a recycling process for Li-ion batteries. *J. Power Sources* **207,** 173–182 (2012).
10. Xu, J. *et al.* A review of processes and technologies for the recycling of lithium-ion secondary batteries. *J. Power Sources* **177,** 512–527 (2008).
11. Shin, S. M., Kim, N. H., Sohn, J. S., Yang, D. H. & Kim, Y. H. Development of a metal recovery process from Li-ion battery wastes. *Hydrometallurgy* **79,** 172–181 (2005).
12. Chen, L. *et al.* Process for the recovery of cobalt oxalate from spent lithium-ion batteries. *Hydrometallurgy* **108,** 80–86 (2011).
13. Nan, J., Han, D., Yang, M., Cui, M. & Hou, X. Recovery of metal values from a mixture of spent lithium-ion batteries and nickel-metal hydride batteries. *Hydrometallurgy* **84,** 75–80 (2006).
14. Narasimha, M., Prasad, V., Maria, H. & Freitas, D. O. Metal hyperaccumulation in plants - Biodiversity prospecting for phytoremediation technology. *Electron. J. Biotechnol.* **6,** 286–321 (2003).
15. Vandenhove, H. & Hees, M. Phytoextraction for clean-up of low-level uranium contaminated soil evaluated. *J. Environ. Radioact.* **72,** 41–45 (2004).
16. American Chemical Society. *Production of aluminium metal by electrochemistry*. (1997).
17. Bhagat, R., Jackson, M., Inman, D. & Dashwood, R. Production of Ti–W Alloys from Mixed Oxide Precursors via the FFC Cambridge Process. *J. Electrochem. Soc.* **156,** E1–E7 (2009).
18. Segws, L., Fontana, A. & Winand, R. Electrochemical boriding of iron in molten salts. *Electrochim. Acta* **36,** 41 (1991).
19. Kartal, G., Eryilmaz, O. L., Krumdick, G., Erdemir, A. & Timur, S. Kinetics of electrochemical boriding of low carbon steel. *Appl. Surf. Sci.* **257,** 6928–6934 (2011).
20. Treatment, E. S., Bonomi, A., Giess, H., Gentaz, C. & Drize, R. De. Electrochemical boriding of molybdenum in molten salts. *Electrodepos. Surf. Treat.* **1,** 419–427 (1973).
21. Saddeek, Y. B. Structural analysis of alkali borate glasses. *Phys. B Condens. Matter* **344,** 163–175 (2004).
22. Dimitriev, Y. & Kashchieva, E. Glass formation and immiscibility in the TeO2-B2O3-Fe2O3-MnO system. *J. Mater. …* **21,** 3033–3037 (1986).
23. Fathi, R. & Sanjabi, S. Electrodeposition of nanostructured Ni(1−x)Mnx alloys films from chloride bath. *Curr. Appl. Phys.* **12,** 89–92 (2012).
24. Zhang, M. *et al.* Electrochemical formation process and phase control of Mg-Li-Ce alloys in molten chlorides. *J. Rare Earths* **31,** 609–615 (2013).
25. Schwandt, C., Dimitrov, A. T. & Fray, D. J. High-yield synthesis of multi-walled carbon

nanotubes from graphite by molten salt electrolysis. *Carbon N. Y.* **50,** 1311–1315 (2012).
26. Bale, C. W. *et al.* FactSage Thermochemical Software and Databases. *Calphad J.* **62,** 189–228 (2002).
27. Amietszajew, T., Seetharaman, S. & Bhagat, R. The Solubility of Specific Metal Oxides in Molten Borate Glass. *J. Am. Ceram. Soc.* 1–4 (2015). doi:10.1111/jace.13801
28. Williams, D. E., Nobile, A. A. & Inman, D. Solvent extraction with inorganic liquids at high temperature. *Trans. I.M.M.* **86,** C35–C37 (1977).
29. Shin, H.-S., Hur, J.-M., Jeong, S. M. & Jung, K. Y. Direct electrochemical reduction of titanium dioxide in molten lithium chloride. *J. Ind. Eng. Chem.* **18,** 438–442 (2012).
30. Stafford, C. R. & Haarberg, C. M. The electrodeposition of Al-Nb alloys from chloroaluminate electrolytes. *Plasmas Ions* **1,** 35–44 (1999).
31. Kawamura, H. & Moritani, K. Discharge electrolysis in molten chloride: formation of fine silver particles. *Plasmas Ions* 29–36 (1998). doi:10.1016/S1288-3255(99)80004-5
32. Liu, Y. *et al.* Electroseparation of thorium from ThO2 and La2O3 by forming Th-Al alloys in LiCl-KCl eutectic. *Electrochim. Acta* (2015). doi:10.1016/j.electacta.2015.01.128
33. Baughman, R., Lefever, R. & Wilcox, W. Evaporation of sodium chloride melts. *J. Cryst. Growth* **8,** 317–323 (1971).
34. Rowell, H. Liquid-Liquid Extraction in the Sodium Oxide-Boron Oxide-Sodium Chloride System. *Inorg. Chem.* **4,** 1802–1806 (1965).
35. Blander, M. *Thermodynamic properties of molten-salt solutions*. (Oak Ridge National Laboratory, 1962). doi:10.1007/978-94-009-3863-2_2
36. Wisniak, J. Borax, boric acid, and boron - From exotic to commodity. *Indian J. Chem. Technol.* **12,** 488–500 (2005).
37. Westphal, G. *et al.* in *Ullmann's Encycl. Ind. Chem.* (Wiley-VCH Verlag GmbH & Co. KGaA, 2000). doi:10.1002/14356007.a24_317.pub4
38. Kamberovic, Z., Korac, M., Ivsic, D., Nikolic, V. & Ranitovic, M. Hydrometallurgical Process for Extraction of. *Metall. Mater. Eng.* **15,** 231–243 (2009).
39. Kang, H. Y. & Schoenung, J. M. Economic analysis of electronic waste recycling: Modeling the cost and revenue of a materials recovery facility in California. *Environ. Sci. Technol.* **40,** 1672–1680 (2006).
40. Marcus, Y. Volumetric behavior of molten salts. *Thermochim. Acta* **559,** 111–116 (2013).
41. Donne, M. D. & Dorner, S. Measurements of Density and of Thermal Expansion Coefficient of Sodium Tetraborate (Borax)-UO2 Solutions. (1980).
42. Greenwood, N. N. & Earnshaw, A. *Chemistry of the Elements*. (1997).
43. Xu, Q., Schwandt, C. & Fray, D. J. Electrochemical investigation of lithium and tin reduction at a graphite cathode in molten chlorides. *J. Electroanal. Chem.* **562,** 15–21 (2004).
44. Vonau, W., Oelßner, W., Guth, U. & Henze, J. An all-solid-state reference electrode. *Sensors Actuators B Chem.* **144,** 368–373 (2010).
45. Wen, Y. & Wang, X. Characterization and application of a metallic tungsten electrode for potentiometric pH measurements. *J. Electroanal. Chem.* **714-715,** 45–50 (2014).
46. Su, L., Liu, K., Liu, Y., Wang, L. & Yuan, L. Electrochemical behaviors of Dy (III) and its co-reduction with Al (III) in molten LiCl-KCl salts. *Electrochim. Acta* **147,** 87–95 (2014).
47. Lewenstam, A. & Scholz, F. *Handbook of Reference Electrodes*. (Springer Berlin Heidelberg, 2013). doi:10.1007/978-3-642-36188-3
48. Fisher, A. C. *Electrode Dynamics*. (Oxford University Press, 2006).
49. Nicholson, R. S. Theory and Application of Cyclic Voltammetry for Measurement of Electrode Reaction Kinetics. *Anal. Chem.* **37,** 1351–1355 (1965).
50. Haarberg, G. M., Støre, T. & Tunold, R. Metal deposition from chloride melts : I . Rates of diffusion in solvent melt. *Electrochmica Acta* **76,** 256–261 (2012).
51. Leng, Y. *Materials Characterization*. (Wiley-VCH, 2013).
52. Bard, A. & Faulkner, L. *Electrochemical methods: fundamentals and applications*. (John Wiley

& Sons, Inc., 1980).
53. Gaur, H. & Jindal, H. Standard electrode potentials in molten chlorides—II. *Electrochim. Acta* **15,** 1113–1126 (1970).
54. Lovering, D. G. *Molten Salt Technology*. (Springer Science + Business Media New York, 1982). doi:10.1007/978-1-4757-1724-2
55. Dunicz, B. L. & Scheidt, R. C. Immiscibility Diagrams of Molten Sodium Chloride - Sodium Polyborates at 810 and 980 C. *J. Chem. Eng. Data* **11,** 566–570 (1966).
56. Shevelin, P. Y., Molchanova, N. G., Yolshin, a. N. & Batalov, N. N. Electron transfer in an electron–ion molten mixture of CuCl–CuCl2–MeCl (Me=Li, Na, K, Cs). *Electrochim. Acta* **48,** 1385–1394 (2003).
57. Martínez, A. & Børresen, B. Electrodeposition of magnesium from the eutectic LiCl–KCl melt. *J. Appl. Electrochem.* **34,** 1271–1278 (2004).
58. Hills, G. J., Schiffrin, D. J. & Thompson, J. Electrochemical Nucleation From Molten Salts 1. Diffusion Controlled Electrode Position of Silver From Alkali. *Electrochim. Acta* **9,** 657–670 (1974).